Materials Sciences and Applications, **2014, 5, 1-9**
Published Online January 2014 (http://www.scirp.org/journal/msa)
http://dx.doi.org/10.4236/msa.2014.51001

Electronic Properties of Nanopore Edges of Ferromagnetic Graphene Nanomeshes at High Carrier Densities under Ionic-Liquid Gating

Taijyu Hashimoto, Syota Kamikawa, Yuko Yagi, Junji Haruyama*

Faculty of Science and Engineering, Aoyama Gakuin University, Sagamihara, Japan.
Email: *J-haru@ee.aoyama.ac.jp

Received November 21st, 2013; revised December 20th, 2013; accepted December 31st, 2013

ABSTRACT

Graphene edges with a zigzag-type atomic structure can theoretically produce spontaneous spin polarization despite being a critical-metal-free material. We have demonstrated this in graphene nanomeshes (GNMs) with honeycomb-like arrays of low-defect hexagonal nanopores by observing room-temperature ferromagnetism and spin-based phenomena arising from the zigzag-pore edges. Here, we apply extremely high electric fields to the ferromagnetic (FM) GNMs using an ionic-liquid gate. A large on/off-ratio for hole current is observed for even small applied ionic-liquid gate voltages (V_{ig}). Observations of the magnetoresistance behavior reveal high carrier densities of ~10^{13} cm^{-2} at large V_{ig} values. We find a maximum conductance peak in the high $-V_{ig}$ region and its separation into two peaks upon applying a side-gate (in-plane external) voltage (V_{ex}). It is discussed that localized edge-π band with excess-density electrons induced by V_{ig} and its spin splitting for majority and minority of spins by V_{ex} (half-metallicity model) lead to these phenomena. The results must realize critical-element-free novel spintronic devices.

KEYWORDS

Graphene; Nanomesh; Edge; Spin Polarization; Magnetism; Ionic-Liquid Gate; High Electric Fields; Rare-Metal-Free Spintronics

1. Introduction

The presence of spontaneously spin-polarized electrons has been theoretically reported at zigzag-atomic structure of edges of graphenes with flat energy bands [1-3]. We experimentally reported it at the hydrogen (*H*)-terminated pore edges of low-defect graphene nanomeshes (GNMs: **Figure 1(a)**) [1-15], which were fabricated using non-lithographic method (*i.e.*, nanoporous alumina templates as etching masks [11]), by observing the ferromagnetism (*i.e.*, ferromagnetic GNMs (FM-FNMs)) [1-9], the distribution of the polarized edge spins by magnetic force microscope [10], and some spin-based phenomena [10-15]. The spin polarization appeared because of the low-defect zigzag atomic structure of the pore edges [1-7] formed by edge reconstruction caused by critical-temperature annealing [12-14] and the assembly of narrow interpore regions (e.g., 10 ~ 20 nm width) corresponding to *H*-terminated zigzag graphene nanoribbons (GNRs: one-dimensional strip lines of graphene with edges on both longitudinal sides; **Figure 1(a)** [8,9]). A large ensemble of GNRs in a GNM enabled the emergence of large-magnitude ferromagnetism even at room temperature.

On the other hand, recently, several studies have reported achieving extremely high carrier densities on material surfaces (e.g., observing the transition from insulators to superconductors and carrier filling in higher energy bands) using electrolytic gates (e.g., ionic liquids and ionic solid-polymers: **Figures 1(c)** and **(d)**) [16-23]. The method enables the realization of a drop in the electric

*Corresponding author.

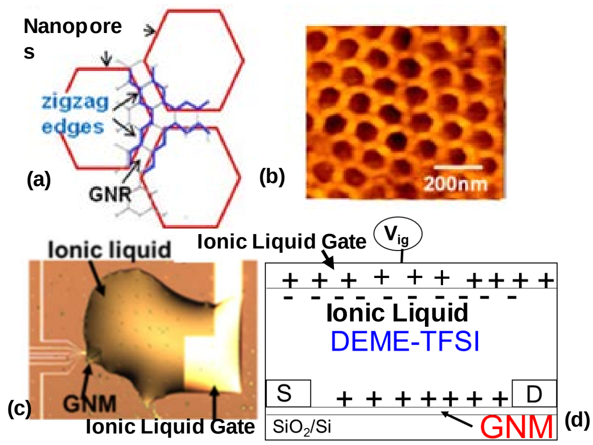

Figure 1. Sample structures (a) Schematic top-view and (b) atomic force microscope image of hydrogen (*H*)-terminated zigzag GNMs, which gives a honeycomb-like array of low-defect hexagonal nanopores. The mean pore diameter and interpore distance are ~80 nm and ~20 nm, respectively. The interpore regions can be *H*-terminated graphene nanoribbons (GNRs) with a width of ~20 nm and, thus, the GNM can be a large ensemble of *H*-terminated-zigzag GNRs, resulting in the appearance of large ferromagnetism. (c),(d) Hall-measurement pattern of the ~5-layer ferromagnetic (FM) GNM with an ionic-liquid gate using DEME-TFSI [19]. Side-gate electrode, which is located within ~500 μm distance from the GNM and is not covered by ionic liquid, was used for applying V_{ex}.

field only at the interface of the material surface (e.g., only for a thickness of 1 nm) via the formation of a Debye layer (Figure 1(d)), thereby resulting in the concentration of an extremely high electric field at the surface. The method has been also applied to graphenes. For example, high carrier densities obtained by this method ($\gg 10^{14}$ cm^{-2}) have revealed the presence of the quantum distribution of two-dimensional (2D) acoustic phonons in graphenes. Further, the filling of the high-energy subbands has been observed along with high electron mobility in bilayer graphenes [16,17]. These results indicate the importance of the high carrier densities observed in graphenes (edges) in the light of examining novel electronic states and physical phenomena.

Indeed, a variety of spin-related phenomena have been predicted based on the study of the edge spins of graphene [6,24-28]. For instance, half-metallicity was predicted in GNRs with antiferromagnetic (AF) spin alignment at two zigzag edges [6]. In such a GNR, the gap for the spins with the same moment (e.g., up spins) between both edges disappears upon applying in-plane external electric fields (V_{ex}), while the gap for the opposite-moment spins (e.g., down spins) increases. The occurrence of the (quantum) spin Hall effect was also predicted by resolving the double degeneration of edge spin bands (e.g., by introducing spin-orbit interactions) and controlling two spins with opposite moments existing in two different bands by applying electric fields [25,26]. In this light, a large spin current was experimentally observed using Zeeman splitting in high-quality bulk graphenes positioned on h-boron-nitride (BN) [27]. We have also reported possible spin-based phenomena arising from the pore edges of ~5-layer FM-GNMs [28].

In the present study, we fabricate an ionic-liquid gate on ~5-layer FM-GNMs with polarized spins at the pore edges, and we observe the changes in the pore-edge electronic and spintronic states induced by the applied ionic-liquid gate voltage V_{ig} and also the side-gate voltage V_{ex} via an electrode not connected to the ionic liquid.

2. Experimental Results and Discussions

2.1. Sample Fabrication

Figure 1 shows the top-view schematic (a) and atomic force microscope images (b) of H-terminated zigzag GNMs and the optical microscope image of the Hall-measurement pattern on the fabricated GNM with an ionic-liquid gate (c), (d). The GNMs, which have honeycomb-like array of hexagonal nanopores, were fabricated on mechanically exfoliated graphenes via the non-lithographic method using a nano-porous alumina template (NPAT) as an etching mask [10,11].

The NPAT is easily fabricated through self-organization by anodic oxidation of pure (99.99%) aluminum films. The graphene was carefully etched by optimized low-power Ar gas (e.g., 200 - 600 V for 10 - 40 min) so as to avoid giving damages (Figure 1(d)) and the naomesh of the NPAT was transferred to graphene. Then, the NPAT was detached from the surface of the fabricated GNM, either mechanically or chemically.

The GNMs fabricated through these processes were annealed at a critical temperature 800˚C in high vacuum (10^{-6} Torr) for 0.5 - 3 days with continual pumping of gas and, then, in hydrogen gas by the field-emission-type radical CVD system under pressure >1 MPa at least for 3 h. The first annealing is for deoxidization of the pore edges with recovering all damages and defects and is the key to forming zigzag pore edges by edge atomic reconstruction [10,12-14], while the second annealing is the key for termination of the carbon atoms at the pore edges by hydrogen atoms for production of flat-band ferromagnetism.

It is to be noted that for electrical measurements, we employed ~5-layer graphenes, because monolayer GNMs exhibited poor electrical features. We have previously confirmed that even such thin-layer GNMs can exhibit ferromagnetism comparable with that of monolayer GNMs, although the amplitude reduces [1-3,22,23]. In fact, we have performed electrode fabrication and measurements after the confirmation of presence of the ferromagnetism.

The ionic-liquid gate was formed to apply V_{ig} following ref. [19] by dropping N, N-diethyl-N-(2-methoxyethyl)-N-methylammonium bis-(trifluoromethylsulfonyl)-imide (DEME-TFSI) (**Figures 1(c)** and **(d)**). Applied V_{ig} is consumed on at the interface of ionic liquid and the GNM, forming electrical-double layer within ~1 nm thickness (**Figure 1(d)**). Thus, it induces extremely high electric fields on the GNM surface. In the present experiment, side-gate electrode not exposed to the ionic liquid was used to apply the V_{ex}.

2.2. Changes in Electrical Properties and Extremely Large $I_{on/off}$ upon V_{ig}

Figure 2 shows the drain current (I_{ds}) as a function of the back-gate voltage (V_{bg}) and V_{ig} (*i.e.*, before and after the formation of the ionic-liquid gate). Without the ionic-liquid gate, the FM-GNM exhibits only n-type semiconductive behavior; I_{ds} increases only with increasing V_{bg} (**Figure 2(a)**). I_{ds} is zero even when V_{bg} is as small as −20 V. In contrast, with the ionic-liquid gating, I_{ds} drastically increases with decreasing V_{ig} (**Figure 2(c)**). Even when V_{ig} is ~ −1 V, the p-type semiconductive behavior appears significantly. This can be attributed to hole doping by the partial oxygen-termination of the pore edges. Immediately before forming the ionic-liquid gate, the GNMs were exposed to an air atmosphere, because it is impossible to form the gate in high vacuum or a hydrogen atmosphere. Because the GNM is not covered by any passivation films, the pore edges are easily oxidized through this process, thereby resulting in the partial oxygen-termination and hole doping. Applying $-V_{ig}$ significantly enhances this hole doping via pore edges. This occurrence is different from the case of bulk graphene without edges. Otherwise, the ionic-liquid gate itself might cause oxygen-like termination.

Figures 2(b) and **(d)** show the logarithmic scales of I_{ds} transformed from **Figures 2(a)** and **(c)**. The subthreshold slope values (V_{sub}) are 5 V/decade for increasing I_{ds} in the $+V_{bg}$ region (**Figure 2(b)**) and 270 mV/decade for increasing I_{ds} in the $-V_{ig}$ region (**Figure 2(d)**). The V_{sub} value reflects the on-off ratio of I_{ds} ($I_{on/off}$) for the applied gate voltages and, hence, it is extremely important for field-effect transistor (FET) operation. The large $I_{on/off}$ value directly leads to a high gain in the radio-frequency (RF) operation of FETs. The V_{sub} is inversely proportional to the $I_{on/off}$. Previously, we have reported on the electrical characteristics of high-quality and low-defect GNRs derived from the unzipping of carbon nanotubes (CNTs) combined with three-step annealing [8]. These GNR-FETs exhibited a large V_{sub} of 3 V/decade for a 20-nm width. The GNMs derived using polymer masks also exhibited a large V_{sub} of ~3 V/decade for a 7-nm interpore width (*i.e.*, GNR width) [29]. Only the GNRs obtained from the unzipping of CNTs exhibited a small V_{sub} of 210 mV/decade but for a 2-nm width [9]. Thus, the present V_{sub} of 270 mV/decade for the 20-nm interpore width is extremely small compared with those of any other GNR-FETs. This strongly suggests the effectiveness of ionic-liquid gating in producing and modulating extremely high electric fields on the GNM surface and the interpore GNR regions.

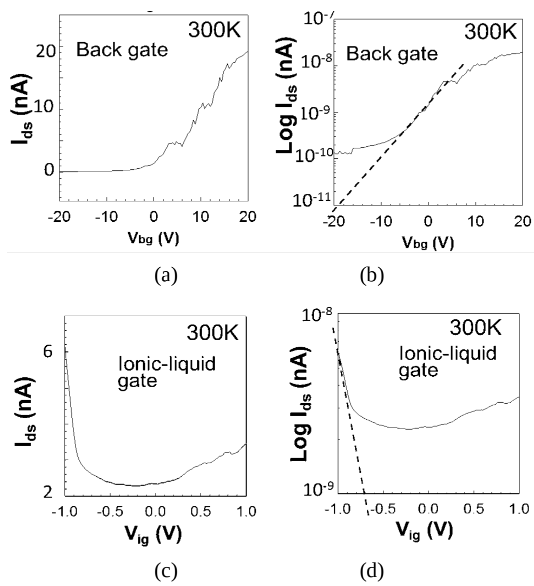

Figure 2. Electrical characteristics of GNM with back gate and ionic-liquid gate (a) Drain current (I_{ds}) as a function of back-gate voltage (V_{bg}) and (b) its transformation to the logarithmic scale of I_{ds} of the ~5-layer FM-GNMs. The GNMs show n-type semiconductive behavior and subthreshold slope values (V_{sub}) of 5 V/decade. (c) I_{ds} as a function of ionic-gate voltage (V_{ig}) after formation of the ionic gate and (d) its transformation to the logarithmic scale of I_{ds}. A drastic increase in I_{ds} in the $-V_{ig}$ region, indicative of p-type behavior, is observed with V_{sub} as small as 270 mV/decade.

2.3. Estimation of Carrier Densities by Magnetoresistance Observation and Large Geometrical Capacitance of Ionic-Liquid Gate

We investigate the charge density n_s achieved upon applying V_{ig} by observing the magnetoresistance (MR) behaviors in the FM-GNMs.

When magnetic fields (B) are applied perpendicular to the GNM plane, the electrons follow a cyclotron motion with the classical radius of the cyclotron orbit, $R_c = (\pi n_s)^{1/2}\hbar/eB$, where h and e denote Planck's constant and the electron charge, respectively [28]. A variety of interesting MR phenomena has been observed depending on the correlation of $2R_c$ with ϕ (the pore diameter) and a (the diameter of the unit cell). For instance, commensurability MR peaks and Aharonov-Bohm (AB)-type oscillations (with an oscillation period $B_{ABT} = (h/e)/S$, where S denotes the area of the unit cell) were observed around low B values at points where electrons encircle and localize around the nanopores (see **Figure 3(a)**; $2R_c = a$) for samples with large ϕ/a values and small interpore spacing (*i.e.*, $2(a - \phi)$) that is insufficient to allow electron cyclotron motion. In contrast, at high B values, Shubnikov-de Haas (SDH) oscillations and consequent quantum Hall effects appeared for samples with small ϕ/a values and large interpore spacing that allowed for electron cyclotron motion with the small Rc values.

In a previous work on FM-GNMs with nearly identical structure parameters as those in the present one but without the ionic-liquid gate, a commensurability MR peak was observed at B ~ 1.2 T [28]. From the expression $2R_c = 2(\pi n_s)^{1/2}\hbar/eB = a$, we estimated $n_s \approx 4\times10^{11}\,\mathrm{cm}^{-2}$ and an elastic mean free path of $\ell_e = 2D/v_F$ (where D denotes the diffusion constant and v_F denotes the Fermi velocity) ~800 nm. Based on this result, we can estimate n_s under extremely high electric fields caused by applying V_{ig} to FM-GNMs with an ionic-liquid gate.

Figure 3 shows the MR (R_{xx}) as a function of V_{ig}. The commensurability MR peak can be observed at B ~ 1 T at V_{ig} = 0 V. As V_{ig} decreases, the peak shifts to larger B regions. The maximum peak position of B ~ 5 T is observed at V_{ig} = −12 V. This indicates an increase in n_s with decreasing V_{ig}, because a large n_s value requires a large B value in order to satisfy the condition for the commensurability peak: $2R_c = a$. Consequently, the maximum n_s of ~$1 \times 10^{13}\ \mathrm{cm}^{-2}$ can be estimated from the peak B value for V_{ig} = −12 V.

This value is extremely large despite the small value of the assembled 20-nm-width GNR structure of the present GNM. This large value is attributed to the large electric field caused by V_{ig}. Moreover, this result also implies the contribution of the induced edge-π states of the nanopores, in which high-density carriers localize at the pore edges even when B = 0 (*i.e.*, the large peak around V_{ig} = −12 V in **Figure 4(b)**, explained later). These edge-localized carriers are added to the cyclotron elec- trons at V_{ig} = −12 V, thereby resulting in extremely large values of n_s. Indeed, it is noteworthy that the peak position moves to a lower B value and n_s decreases at V_{ig} = −16 V. This evidences the contribution of the edge-π electrons localized around the pore at V_{ig} = −12 V. Fur- thermore, the extremely large n_s value results in a small mean free path (l_e) of ~800 nm, which is considerably smaller than the circumferential length of the pore and cell (~250 nm). Thus, the present GNM is not within a ballistic charge transport regime, and no AB-type oscillations are observed in **Figure 3(b)**.

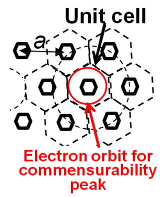

(a)

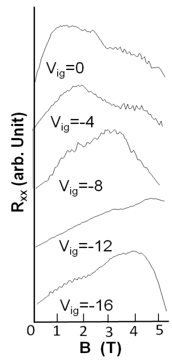

(b)

Figure 3. Magnetoresistance behavior for various ionic-liquid gate voltages (a) Schematic view of an electron orbit for a commensurability MR peak in a GNM. The peak appears at a *B* value where the electron cyclotron diameter ($2R_c$) is close to the unit cell diameter (a) and electrons localize in the unit cell. (b) MMR behavior (R_{xx}) in a perpendicular field as a function of V_{ig} of FM-GNMs with ~5-layers at T = 1.5 K. The broad MR peaks at each V_{ig} value indicate the commensurability MR peaks mentioned in (a). Change in the peak position is caused by the modulation of n_s upon changing V_{ig}. The peak *B* positions provide the n_s values of the FM-GNM at each V_{ig}, which includes the pore-edge localized electrons even for *B* = 0.

In addition to the extremely high value of n_s, the other strong advantage of using the ionic-liquid gate is the obtainment of a large geometrical capacitance (C_{geo}) [19], which allows the direct observation of the quantum capacitance (C_Q). The large geometry of the ionic-liquid region (**Figure 1(c)**) provides an extremely large C_{geo}. This capacitance allows the direct observation of the quantum capacitance ($C_Q = e^2 D_{2D} = m^*/\pi h^2$, where m^* denotes the effective mass of carriers and D_2 is the electronic density of states of the 2D layer), because the total capacitance is given by $1/C_{tot} = 1/C_{geo} + 1/C_Q$ and the $1/C_{geo}$ value is negligible. In fact, a previous work has reported on the possible detection of D_{2D} at higher energy bands arising from the C_Q of individual layers in monolayer to trilayer graphenes, using this method. Here, the capacitance of 2D systems is conventionally obtained from the Hall measurements (*i.e.*, changes in n_s as a function of $V_g : C_{geo} = e(\mathrm{d}n_s/\mathrm{d}V_g)$). However, it is difficult to employ this method in our case because the scattering by the honeycomb-like nanopore array prevents Hall measurements.

Instead, we employ a GNR model in order to estimate C_{geo}, and reconfirm the possibility of the direct observation of C_Q, because the interpore regions are GNRs (**Figure 1**). The GNR models gives carrier mobility $\mu = g_m L / C_{geo} V_{ds}$, where g_m denotes the mutual conductance and L denotes the GNR length8. The g_m value of ~500 mS at V_{ds} = 0.8 V is observed in **Figure 2(d)**, and L corresponds to the inter-electrode distance of 2500 nm in our fabricated GNM. In a previous report, we have also estimated μ < ~100 cm^2/Vs in FM-GNMs from MR measurements [28]. Consequently, C_{geo} for the side gate electrode is estimated to be ~12 $\mu F/cm^2$.

This value is in good agreement with those in previous reports on ionic-liquid (electrolytic) gates [19]. Conventional GNRs with widths of 2 ~ 20 nm placed on SiO_2 substrates have C_{geo} ~ 10^{-10} - 10^{-12} F for the source electrodes. Thus, the present C_{geo} value is nearly 10^5 times greater than these reported values. Therefore, we can estimate C_Q and D_{2D} directly from the measurement results related to C_{tot} also in our GNM.

2.4. Observation of Differential Conductivity on V_{ig}

Figure 4(a) shows the differential conductivity (d*I*/d*V*; R_{xx}^{-1}) as a function of V_{ig} in the low-V_{ig} region when B = 0 T. Even in the present ~5-layer GNM, a Dirac-point-like dip (zero-bias anomaly) is observed in the d*I*/d*V* curves. Moreover, as the absolute value of V_{ig} increases, other dips and peaks appear. Such d*I*/d*V* anomalies due to V_{ig} variation have been reported in tri-layer graphenes with ionic-liquid gates and attributed to carrier filling in higher energy bands (*i.e.*, interband scattering). This is a advantage unique to the electrolytic gate method for the abovementioned reasons (*i.e.*, introducing large electric fields and the presence of a large C_{geo}). The curves in **Figure 4(a)** are qualitatively consistent with the abovementioned features. However, in **Figure 4(a)**, the d*I*/d*V* anomalies observed at V_{ig} ~ ±0.3 V are considerably more defined than those observed in the tri-layer graphenes. Moreover, the plateau of the second peak in the +V_{ig} region is broad and consists of very small peaks. The presence of these peaks might suggest very strong interband scattering and the presence of a complicated higher-band structure in our ~5-layer FM-GNM.

In the large V_{ig} region (**Figure 4(b)**), we observe many d*I*/d*V* peaks. In particular, a significantly large and broad d*I*/d*V* peak is observable around V_{ig} ~ −12 V, when the side-gating V_{ex} is 0 V (dotted line in **Figure 4(b)**). Although the d*I*/d*V* properties as a whole are very complicated, the observed large d*I*/d*V* values in the -V_{ig} region at V_{ex} = 0 V are consistent with the hole-dominant property in **Figures 2(c)** and **(d)**. This consistency indicates

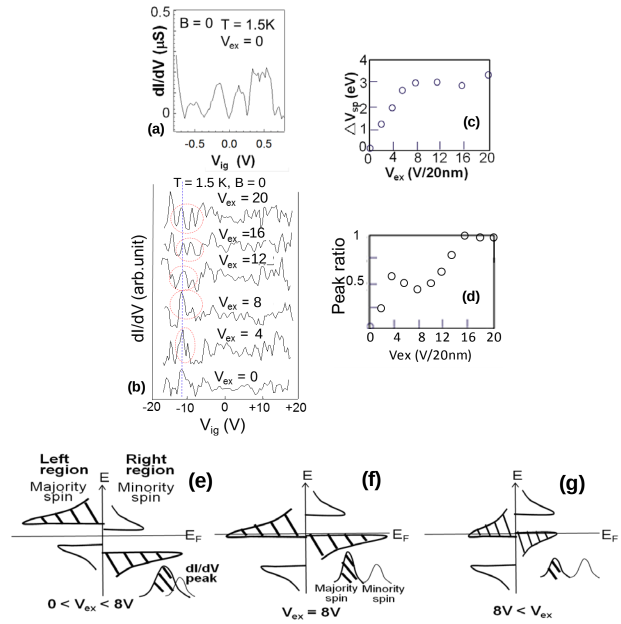

Figure 4. Conductivity behaviors for various ionic-liquid gate voltages V_{ig} and side-gate (in-plane external) voltages V_{ex} (a) Differential conductivity (d*I*/d*V*) as a function of V_{ig} at low V_{ig} values. (b) d*I*/d*V* curves in the high-V_{ig} regions with side-gating V_{ex}. The dashed vertical line indicates the location of the maximum peak and the dashed circle indicates its splitting into two peaks with increasing V_{ex}. (c) The spin splitting voltage ΔV_{ig} estimated from the two peaks in Figure 4(b) as a function of side-gate V_{ex}. (d) Peak ratio for left/right peaks as a function of V_{ex} in Figs.4b and 4c. It should be noticed that the peak ratio starts to significantly increase from the critical V_{ex} ~ 8 V due to the reduction in the height of the left peak, at which point ΔV_{ig} saturates in Figure 4(c). (e)-(g) Hal-metallicity-based schematics of changes in spin bands for majority and minority spins at both edges of a FM-GNR (corresponding to the interpore region) as a function of the in-plane V_{ex}. Insets: The schematics of the two dI/dV peaks shown in Figure 4(b).

the significant appearance of p-type semiconductive behavior.

The d*I*/d*V* values typically have a strong correlation with D_{2D} and n_s, conventionally. A large D_{2D} value around Fermi level results in a large d*I*/d*V* value [16,17]. Hence, the maximum d*I*/d*V* peak around V_{ig} ~ −12 V (**Figure 4(b)**) should reflect the maximum D_{2D} value of our FM-GNM.

Because the edge-localized flat π band has the largest D_{2D} values (edge states) and strongly contributes to the appearance of the ferromagnetism also in graphites [3, 21-23], the maximum d*I*/d*V* peak should correspond to this edge-π band. Theoretical works have proposed that the edge-magnetic moment arising from the edge-π state survives even in graphites with interlayer interaction (e.g., ABA stacking with mono-hydrogenated edges) [3,21-23]. Moreover, because the present FM-GNM has only ~5-

layers, the influence of interlayer coupling for suppressing the emergence of ferromagnetism is very weak.

However, the localization of the edge-electrons prohibits current flow and obstructs detection of the large D_{2D} by d*I*/d*V* observation in the present case, even if the D_{2D} value is very high. Nevertheless, we have reported certain MR behaviors (e.g., periodic MR oscillations [28] and saw-tooth-like MR oscillations [10]) originating from edge-localized π-electrons in similar ~5-layer FM-GNMs operating under a constant current mode in four-probe measurements. We have argued that certain numbers of pore-edge-localized electrons can travel between electrodes because of the constant current mode (*i.e*., under non-thermal equilibrium). Moreover, the n_s value of ~1×10^{13} cm^{-2} around V_{ig} ~ −12 V observed in our ionic-liquid-gated FM-GNMs is considerably larger than the n_s value of conventional FM-GNRs. This result supports the strong contribution of the drastically induced pore-edge π-electrons, as mentioned above. In such a case, the excess π-electrons localizing at the pore edges can be transported considerably more efficiently under a non-thermal equilibrium condition and contribute to the d*I*/d*V*. Therefore, we can assume that the maximum d*I*/d*V* value directly reflects the edge-localized π band with the highest DOS via the excess π electrons, as seen from scanning tunnel microscopy observations of the DOS.

Such maximum d*I*/d*V* peaks cannot be observed in conventional electrolytic-gated bulk graphenes without nanopores (*i.e*., without edge states), which showed no FM behavior, and such behavior has not thus far been observed in measurements obtained by applying V_{bg}. These results strongly support the correlation of the observed maximum d*I*/d*V* peak with the induced pore-edge π-electrons in our ionic-liquid gated ~5-layer FM-GNMs.

On the other hand, several other d*I*/d*V* peaks are also observed in **Figure 4(b)**. These should originate from other D_{2D} states, which are sensitive to spin interference by 1) the spin alignment of both the edges of the interpore GNR regions [3], 2) large ensemble of the GNR regions, 3) the interlayer stack structures [22], and also 4) V_{ig} and V_{ex}. Thus, it is difficult to identify the origins of the individual peaks. For example, the second-largest peaks observed around V_{ig} ~ −5 V and −12 V at V_{ex} = 0 in **Figure 4(b)** may be associated with the *σ* band, because the present GNMs have ~5-layer. In the present work, we focus on the largest d*I*/d*V* peak observable around V_{ig} ~ −12 V at V_{ex} = 0 in **Figure 4(b)**, because **Figures 4(b)-(d)** suggest its strong correlation with the edge-π band, as stated in next section.

2.5. Splitting of a Maximum Conductance Peak by In-Plane External Fields and Half-Metallicity Model

As mentioned above, we interestingly find that the maximum d*I*/d*V* peak around V_{ig} ~ −12 V separates into two peaks upon increasing the V_{ex} (**Figure 4(b)**). The splitting voltage ΔV_{ig} monotonically increases with increasing V_{ex} and saturates at around V_{ex} = 8 V with ΔV_{ig} ~ 3 eV (**Figure 4(c)**). At low values of V_{ex}, the left peak is considerably more prominent than the right peak (**Figure 4(b)**), while the left peak height reduces for large V_{ex} values, and eventually, the two peaks exhibit similar heights. The peak ratio for the left/right peaks after peak separation becomes equal with increasing V_{ex} because of the decrease in the left-peak height (**Figure 4(d)**).

This spin splitting can be qualitatively understood by the resolving of the double spin degeneration of the edge-localized flat π band (*i.e*., separating of the majority- and minority-spin bands, which correspond to the left and right peaks, respectively) by applying the side-gating V_{ex}, which plays role like applying in-plane V_{ex}. Because the contribution of the localized minority-spins to d*I*/d*V* is very small, the right-peak height is actually small throughout all the V_{ex} regions (**Figure 4(b)**). Indeed, such a spin splitting upon the application of an electric field has been reported as an anomalous spin Hall effect in FM/non-FM hybrid materials (e.g., Pt/Ni-Fe). From the theoretical viewpoint, the presence of spin bands for the majority and minority spins has also been reported in FM-GNRs [3].

One particular theory [6] has predicted the half-metallicity and spin-gap opening that can be realized upon applying the in-plane field V_{ex} in zigzag-GNRs with AF spin alignment at both the edges (as mentioned in the introduction). In our fabricated FM-GNMs, the spin alignment at the two edges of the interpore GNR region is FM. However, when a similar mechanism is realized for the majority and minority spins with opposite moments for FM-GNRs assembled between the electrodes, the above mentioned spin splitting can be observed (**Figures 4(e)-(g)**), and it can be explained by assuming that the side-gate V_{ex} plays the role of the in-plane field V_{ex}. The predicted spin-gap opening as per the theory was Δ_{theory} ~ 0.5 eV for V_{ex} = 0.1 V/Å. In contrast, the abovementioned value of ΔV_{ig} ~ 3 eV for V_{ex} = 8 V corresponds to a considerably larger ΔV_{ig}. As mentioned above, we have used the side-gating voltage V_{ex} for this observation. When V_{ex} = 8 V is applied from the side-gate electrode directly placed on the Si substrate, the voltage propagates via the substrate surface, thereby leading to a potential difference between both sides of the individual interpore GNR with 20-nm width. The potential difference can be estimated to be ~0.1 V/20nm, based on our previous work [8]. Thus, ΔV_{ig} ~ 3 eV for V_{ex} = 8 V corresponds to ΔV_{ig} ~ 600 eV for V_{ex} = 0.1 V/Å. This ΔV_{ig} value is considerably larger than the theoretical prediction Δ_{theory} ~ 0.5 eV.

However, because this value of ΔV_{ig} ~ 600 eV is not the actual spin splitting energy in the GNM but corresponds to the V_{ig} value applied to the side-gate electrode, the actual splitting energy ΔV_{sp} needs to be calculated. The ΔV_{sp} value corresponds to the energy in the single-particle energy spectrum given by

$$\Delta V_{sp} = \hbar v_F \sqrt{2\pi C_{geo} \Delta V_{ig} / |e|}$$

Here, v_F ~ 10^3 m/s denotes the Fermi velocity in our fabricated GNM, which is at least 1000 times smaller than that for bulk graphene [8] considering edge scattering. Using the previously estimated value of C_{geo} ~ 12 μF/cm^2, ΔV_{sp} can be estimated to be ~0.54 eV. This value is quantitatively in good agreement with the abovementioned theoretical prediction of ΔV_{theory} ~ 0.5 eV. This estimation also implies that the edge-localized π band (*i.e.*, the observed d*I*/d*V* peak at V_{ig} ~ −12 V) exists at ~1.2 eV below the initial Fermi level position at V_{ig} = 0 V. Because the FM-GNM consists of the assembled FM-GNRs, this might smear the d*I*/d*V* maximum and also its splitting by averaging. However, we assume that only the dominant some GNRs (interpore regions), of which the width-direction (*i.e.*, both edges) locates in parallel with electrodes to apply V_{ex}, and have perfect zigzag edges, strongly contribute to these phenomena.

Moreover, it should be noticed that the peak ratio starts to significantly increase from the critical V_{ex} value of 8 V due to the reduction in the height of the left peak (**Figure 4(d)**), at which point ΔV_{ig} saturates (**Figure 4(c)**). This result supports the conclusions of the half-metallicity model [6]. Following this model, the saturation of ΔV_{ig} corresponds to the gap closing for one-moment spins existing at both edges of the GNRs (**Figure 4(f)**). Although this gap closing facilitates the same-moment spin current flow across the GNR, the localization of the edge electrons for the majority spin is suppressed by the spin current flow. A further increase in V_{ex} results in a decrease in the amplitude of the edge states (*i.e.*, resulting in a decrease in the excess n_s) for the same-moment spins and, thus, the left-peak height decreases (**Figure 4(g)**) despite appearance of the current flow.

Consequently, we suggest that the applied side-gate V_{ex} causes spin splitting of the edge-π band (for the majority and minority spins with opposite moments for FM-GNRs) similar to that caused by the application of an in-plane V_{ex} following a theory [6]. This is because extremely large values of the D_{2D}, which originate from the edge states of the nanopores induced by V_{ig}, are highly sensitive to added external fields. In fact, we could observe no such V_{ex}-dependent changes in the electronic states in the absence of V_{ig} (in this case, we applied only the back-gate voltage and, consequently, we could not detect even edge-π states, as in **Figure 4**). Because the present GNM is placed on a SiO_2 film, the side-gating V_{ex} cannot directly modulate the interpore GNR edges. However, when the ionic-liquid gate is formed, the liquid faces the pore edges (*i.e.*, both edges of an interpore GNR) and also the surface of SiO_2 at the pore's inner regions. We speculate that such conditions drastically change the large edge-electronic states even for a small potential difference existing between the two edges of the interpore GNR region caused by the side-gating V_{ex}, and the V_{ex} acts in a manner similar to the actual in-plane field V_{ex}.

2.6. Rapid Degradation of Samples during Electrical Measurements

Subsequent to measurements performed over nearly three days, we observed a degradation of the electrical and magnetic characteristics of the FM-GNM. In particular, the appearance of single-electron charging effect was observed in the current channel region (**Figure 5**).

The staircase-like feature is confirmed in the Ids vs. V_{ds} relationship in **Figure 5**. The inset shows dI_{ds}/dV_{ds} as a function of V_{ds}. It exhibits a periodical oscillation with a period of 180 mV. It is well known that such a phenomenon is understood as the Coulomb staircase, which originates from the charging effect of a single electron in an extremely small dot area with a charging energy of $E_c = e^2/2C_{dot}$ ~ 180 meV, where C_{dot} denotes the capacitance of the dot area [30,31]. The C_{dot} value corresponds to ~10^{-18} F, which is a value that is considerably smaller than C_{geo} and also any other capacitances of the present GNM-FET structure. This result strongly suggests the emergence of small defects in the current channel region due to degradation after the three-day measurements. Indeed, ref. [16] reported on the quick degradation of graphenes with electrolytic gates and the consequent importance of obtaining quick measurements.

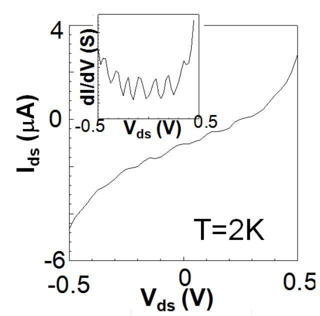

Figure 5. **Electrical characteristics after three-day measurements I_{ds}-V_{ds} relationship after the measurements through nearly three days. The sample was placed in a He-gas atmosphere in a Cryomag system (Oxford Inst.) at T = 1.5 K during the measurements. Inset: dI_{ds}/dV_{ds} as a function of V_{ds}. The curve exhibits a periodical oscillation with a period of 180 mV, the so-called Coulomb staircase.**

The sample was placed under high-vacuum conditions in a Cryomag system (Oxford Instruments) at T = 1.5 K during the measurements. Thus, we concluded that the edge degradation is due to the chemical reaction of the (frozen) ionic liquid with the GNM during the measurement. Because the H-terminated pore edges face the ionic liquid, they are most sensitive to such degradation. In the present edge-related measurements, a more careful treatment of the GNMs will be required, because it is well known that the edge-based phenomena are highly sensitive to edge degradation.

Moreover, in our previous works, we have reported observing AB-type MR oscillations [28] and saw-tooth like MR oscillations (*i.e.*, the spin pumping effect [10]) arising from the localized electrons at the pore edges in ~5-layer FM-GNMs without ionic-liquid gating. On the other hand, in the present structure with ionic-liquid gates, these oscillations are hardly observed. This absence of oscillations might also be due to the partial degradation caused by the chemical reaction between the pore-edge carbon atoms and the ionic liquid.

3. Conclusions

Graphene edges with a zigzag-type atomic structure can theoretically produce spontaneous spin polarization despite being a critical-metal-free material. We previously demonstrated this in GNMs with honeycomb-like arrays of low-defect hexagonal nanopores by observing room temperature ferromagnetism and spin-based phenomena arising from the zigzag-pore edges.

In the present work, we applied extremely high electric fields to the FM-GNMs using an ionic-liquid gate. A large on/off-ratio for hole current was observed for even small applied V_{ig}. Observations of the MR behavior revealed the carrier densities as high as $\sim 10^{13}$ cm^{-2} under large V_{ig} values, despite the assembly structure of narrow GNRs with ~20 nm width. C_{geo} as large as ~12 μF/cm^2 was also estimated. We observed a maximum conductance peak in the high $-V_{ig}$ region and its separation into two peaks upon applying a side-gate V_{ex}. Based on half-metallicity model, it was discussed that the localized edge-π band with excess-density electrons induced by V_{ig} and its spin splitting for majority and minority spins caused by V_{ex} led to these phenomena and that the applied V_{ex} played a role similar to that of the in-plane field V_{ex} under the application of V_{ig}.

The present finding clarify that one can detect the localized edge bands via the excess-density electrons due to V_{ig} by observing conductance and also the spin behaviors of the band within controlled manner by applying side-gate V_{ex}. The results must be valuable for critical-element-free novel spintronic devices.

Acknowledgements

The authors thank Y. Iwasa, K. Fujita, Y. Hashimoto, E. Endo, Y. Iye, S. Katsumoto, M. Yamamoto, S. Tarucha for their technical contribution, fruitful discussions, and encouragement. This work was partly supported by a Grant-in-Aid for Scientific Research (Basic research A: 24241046) under the aegis of MEXT, a Grant for Zero-emission Energy program by Kyoto University, and also an AFOSR grant.

REFERENCES

[1] K. Nakada, M. Fujita, G. Dresselhaus and M. S. Dresselhaus, “Edge State in Graphene Ribbons: Nanometer Size Effect and Edge Shape Depend,” *Physical Review B*, Vol. 54, No. 24, 1996, pp. 17954-17961. http://dx.doi.org/10.1103/PhysRevB.54.17954

[2] M. Fujita, K. Wakabayashi, K. Nakada and K. Kusakabe, “Peculiar Localized State at Zigzag Graphite Edge,” *Journal of the Physical Society of Japan*, Vol. 65, 1996, pp. 1920-1923. http://dx.doi.org/10.1143/JPSJ.65.1920

[3] H. Lee, Y. Son, N. Park, S. Han and J. Yu, “Magnetic Ordering at the Edges of Graphitic Fragments: Magnetic Tail Interactions between the Edge-Localized States,” *Physical Review B*, Vol. 72, No. 17, 2005, Article ID: 174431. http://dx.doi.org/10.1103/PhysRevB.72.174431

[4] R. G. A. Veiga, R. H. Miwa and G. P. Srivastava, “Quenching of Local Magnetic Moment in Oxygen Adsorbed Graphene Nanoribbons,” *The Journal of Chemical Physics*, Vol. 128, 2008, Article ID: 201101. http://dx.doi.org/10.1063/1.2937453

[5] T. Enoki and K Takai, “The Edge State of Nanographene and the Magnetism of the Edge-State Spins,” *Solid State Communications*, Vol. 149, No. 27-28, 2009, pp. 1144-1150. http://dx.doi.org/10.1016/j.ssc.2009.02.054

[6] Y. W. Son, M. L. Cohen and S. G. Louie, “Half-Metallic Graphene Nanoribbons,” *Nature*, Vol. 444, 2006, pp. 347-349. http://dx.doi.org/10.1038/nature05180

[7] L. Yang, C. Park, Y. Son, M. L. Cohen and S. G. Louie, “Quasiparticle Energies and Band Gaps in Graphene Nanoribbons,” *Physical Review Letters*, Vol. 99, No. 18, 2007, Article ID: 186801. http://dx.doi.org/10.1103/PhysRevLett.99.186801

[8] T. Shimizu, J. Haruyama, D. C. Marcano, D. V. Kosinkin, J. M. Tour, K. Hirose and K. Suenaga, “Large Intrinsic Energy Bandgaps in Annealed Nanotube-Derived Graphene Nanoribbons,” *Nature Nanotechnology*, Vol. 6, 2011, pp. 45-50. http://dx.doi.org/10.1038/nnano.2010.249

[9] X. Wang, Y. Ouyang, X. Li, H. Wang, J. Guo and H. Dai, “Room-Temperature All-Semiconducting Sub-10-nm Graphene Nanoribbon Field-Effect Transistors,” *Physical Review Letters*, Vol. 100, No. 20, 2008, Article ID: 206803. http://dx.doi.org/10.1103/PhysRevLett.100.206803

[10] K. Tada, T. Hashimoto, J. Haruyama, H. Yang and M. Chshiev, “Spontaneous Spin Polarization and Spin Pum-

ping Effect on Edges of Graphene Antidot Lattices," *Solid State Physics*, Vol. 249, No. 12, 2012, pp. 2491-2496. http://dx.doi.org/10.1002/pssb.201200042

[11] I. Takesue, J. Haruyama, N. Kobayashi, S. Chiashi, S. Maruyama, T. Sugai and H. Shinohara, "Superconductivity in Entirely End-Bonded Multiwalled Carbon Nanotubes," *Physical Review Letters*, Vol. 96, No. 5, 2006, Article ID: 057001. http://dx.doi.org/10.1103/PhysRevLett.96.057001

[12] X. Jia, M. Hofmann, V. Meunier, B. G. Sumpter, J. Campos-Delgado, J. M. Romo-Herrera, H. Son, Y. Hsieh, A. Reina, J. Kong and M. S. Dresselhaus, "Controlled Formation of Sharp Zigzag and Armchair Edges in Graphitic Nanoribbons," *Science*, Vol. 323, No. 5922, 2009, pp. 1701-1705. http://dx.doi.org/10.1126/science.1166862

[13] Ç. Ö. Girit, J. C. Meyer, R. Erni, M. D. Rossell, C. Kisielowski, L. Yang, C. Park, M. F. Crommie, M. L. Cohen and S. G. Louie, "Graphene at the Edge: Stability and Dynamics," *Science*, Vol. 323, No. 5922, 2009, pp. 1705-1708. http://dx.doi.org/10.1126/science.1166999

[14] Y. M. You, Z. H. Ni, T. Yu and Z. X. Shen, "Edge Chirality Determination of Graphene by Raman Spectroscopy," *Applied Physics Letters*, Vol. 93, No. 16, 2008, Article ID: 163112. http://dx.doi.org/10.1063/1.3005599

[15] B. Krauss, P. Nemes-Incze, V. Skakalova, L. P. Biro, K. von Klitzing and J. H. Smet, "Raman Scattering at Pure Graphene Zigzag Edges," *Nano Letters*, Vol. 10, No. 11, 2010, pp. 4544-4548. http://dx.doi.org/10.1021/nl102526s

[16] D. K. Efetov and P. Kim, "Controlling Electron-Phonon Interactions in Graphene at Ultrahigh Carrier Densities," *Physical Review Letters*, Vol. 105, No. 25, 2010, Article ID: 256805. http://dx.doi.org/10.1103/PhysRevLett.105.256805

[17] D. K. Efetov, P. Maher, S. Glinskis and P. Kim, "Multiband Transport in Bilayer Graphene at High Carrier Densities," *Physical Review B*, Vol. 84, No. 16, 2011, Article ID: 161412(R).

[18] A. Das, A. K. Geim, *et al*., "Monitoring Dopants by Raman Scattering in an Electrochemically Top-Gated Graphene Transistor," *Nature Nanotechnology*, Vol. 3, 2008, p. 210. http://dx.doi.org/10.1038/nnano.2008.67

[19] M. Panzer, *et al*., "Photo-Embossed Surface Relief Structures with an Increased Aspect Ratios by Addition of a Reversible Addition—Fragmentation Chain Transfer Agent," *Advanced Materials*, Vol. 20, No. 16, 2008, p. 3117. http://dx.doi.org/10.1002/adma.200800124

[20] K. F. Mac, *et al*., "Observation of an Electric-Field-Induced Band Gap in Bilayer Graphene by Infrared Spectroscopy," *Physical Review Letters*, Vol. 102, No. 25, 2009, Article ID: 256405. http://dx.doi.org/10.1103/PhysRevLett.102.256405

[21] A. H. R. Pasler, "Interlayer Interactions in Graphite and Carbon Nanotubes," *Chemical Physics*, Vol. 1, No. 18, 1999, p. 4459.

[22] M. Otani, M. Koshino, Y. Takagi and S. Okada, "Intrinsic Magnetic Moment on (0001) Surfaces of Rhombohedral Graphitee," *Physical Review B*, Vol. 81, No. 16, 2010, Article ID: 161403 (R). http://dx.doi.org/10.1103/PhysRevB.81.161403

[23] M. Otani, Y. Takagi, M. Koshino and S. Okada, "Phase Control of Magnetic State of Graphite Thin Films by Electric Field," *Appl*. *Phys*. *Lett*., Vol. 96, No. 24, 2010, pp. 242504.http://dx.doi.org/10.1063/1.3455069

[24] S. Murakami, N. Nagaosa and S. Zhang, "Dissipationless Quantum Spin Current at Room Temperature," *Science*, Vol. 301, No. 5638, 2003, pp. 1348-1351. http://dx.doi.org/10.1126/science.1087128

[25] C. L. Kane and E. J. Mele, "Quantum Spin Hall Effect in Graphene," *Physical Review Letters*, Vol. 95, No. 22, 2005, pp. 226801-226804. http://dx.doi.org/10.1103/PhysRevLett.95.226801

[26] M. J. Schmidt and D. Loss, "Edge States and Enhanced Spin-Orbit Interaction at Graphene/Graphane Interfaces," *Physical Review B*, Vol. 81, No. 16, 2010, Article ID: 165439. http://dx.doi.org/10.1103/PhysRevB.81.165439

[27] D. A. Abanin, S. V. Morozov, L. A. Ponomarenko, R. V. Gorbachev, A. S. Mayorov, M. I. Katsnelson, K. Watanabe, T. Taniguchi, K. S. Novoselov and L. S. Levitov, "Giant Nonlocality near the Dirac Point in Graphene," *Science*, Vol. 332, No. 6027, 2011, pp. 328-330. http://dx.doi.org/10.1126/science.1199595

[28] T. Shimizu, J. Nakamura, K. Tada, Y. Yagi and J. Haruyama, "Magnetoresistance Oscillations Arising from Edge-Localized Electrons in Low-Defect Graphene Antidot-Lattices," *Applied Physics Letters*, Vol. 100, No. 2, 2012, Article ID: 023104. http://dx.doi.org/10.1063/1.3675547

[29] J. Bai, X. Zhong, S. Jiang, Y. Huang and X. Duan, "Graphene Nanomesh," *Nature Nanotechnology*, Vol. 5, 2010, pp. 190-194. http://dx.doi.org/10.1038/nnano.2010.8

[30] H. Grabert and M. H. Devoret, "Single Charge Tunneling," NATO ASI Series B, Vol. 294, Plenum, New York, 1991.

[31] J. Haruyama I. Takesue, T. Hasegawa and Y. Sato, "Coulomb Blockade Related to a Localization Effect in a Single Tunnel-Junction/Carbon-Nanotube System," *Physical Review B*, Vol. 63, No. 7, 2001, Article ID: 073406. http://dx.doi.org/10.1103/PhysRevB.63.073406